The Origin of Chiroptic Amplification in Perylene-Diimide Helicenes

Journal:	*The Journal of Physical Chemistry*
Manuscript ID	jp-2020-11382p.R1
Manuscript Type:	Article
Date Submitted by the Author:	n/a
Complete List of Authors:	Aranda, Daniel; Universidad de Malaga, Physical Chemistry Schuster, Nathaniel; Stanford University, Department of Chemical Engineering Xiao, Xiao; Columbia University, Department of Chemistry Avila Ferrer, Francisco; Universidad de Malaga, Physical Chemistry Santoro, Fabrizio; Istituto di Chimica dei Composti Organo Metallici Consiglio Nazionale delle Ricerche Sezione di Pisa, Nuckolls, Colin; Columbia University, Department of Chemistry; Columbia University, Department of Chemistry

The Origin of Chiroptic Amplification in Perylene-Diimide Helicenes

Daniel Aranda,[1,2] Nathaniel J. Schuster,[3] Xiao Xiao,[3] Francisco J. Ávila Ferrer,[2] Fabrizio Santoro,[1*] and Colin Nuckolls[3*]

[1]CNR-Consiglio Nazionale delle Ricerche, Istituto di Chimica dei Composti Organo Metallici (ICCOM-CNR), SS di Pisa, Area della Ricerca, via G. Moruzzi 1, I-56124 Pisa, Italy.

[2]Departamento de Química Física, Universidad de Málaga, Bulevar Louis Pasteur 31, Málaga 29010, Spain.

[3]Department of Chemistry, Columbia University, New York, New York 10027, USA.

[*]email: fabrizio.santoro@pi.iccom.cnr.it; cn37@columbia.edu

Abstract

Molecules with large chiroptic response in the visible range are key in the design of new efficient chiral optoelectronic devices. It has been recently shown that **NP3H**, a helicene-based nanoribbon with three perylene diimides connected by two naphthalene units, exhibits a huge amplification of the electronic circular dichroism response at 400 nm with respect to **NPDH**, its analogue with only two perylene diimides bridged by a single naphthalene. Here we present that time-dependent density functional theory can reproduce this experimental feature, attributing it to a strong increase of the magnetic transition dipole moments of the involved electronic states in **NP3H**. A more qualitative understanding of the phenomenon is obtained with a number of readily accessible computational tools. Analysis of the difference of the electronic densities of the excited and ground states indicates that the key units for explaining the enhancement in electronic circular dichroism are not the perylene diimides but the idealized double[6]helicene substructure of **NP3H**, formed by naphthalene and the adjacent rings within the

perylene diimides. Such analysis further suggests that the amplification arises from an exciton-like coupling, not possible in **NPDH** where only one [6]helicene subunit exists. Computations on different fragments of **NP3H** and application of simple exciton models provide additional support for this mechanism. These results evidence that this double[6]helicene unit could represent a key core for the design of new chiral conjugated materials with enhanced chiroptical properties in the visible range.

I. Introduction

Helicenes are an important class of polycyclic aromatic compounds, in which benzenes or other aromatics are *ortho*-fused to impart a chiral helical structure.[1-4] They are promising candidates for applications in chiral electronics and optoelectronics because of their unique semiconducting and chiroptical properties.[5-6] However, the full potential of helicenes has not been realized, because there is no simple, yet general, understanding of the specific chemical structures that give rise to enhanced chiroptical properties. For example, axial elongation of carbo[*n*]helicenes (*n* denotes the number of *ortho*-annulated benzene rings) does not lead to significant increases in electronic circular dichroism (ECD).[7] Moreover, fusing multiple helicenes to a π-extended nanographene core can result in red-shifted absorbance, but the overall ECD is not consistently enhanced.[8-13] Therefore, it is essential to develop a broadly applicable molecular design for chiral nanographenes with exceptional chiroptical properties.

In this scenario helicenes based on perylene-3,4,9,10-tetracarboxylic-diimide (PDI) subunits are promising materials.[14-16] We recently discovered that **NP3H**, a helicene-based nanoribbon that incorporates three PDI subunits, exhibits large ECD amplification with respect to **NPDH**, its smaller analogue (Figure 1).[14.15]

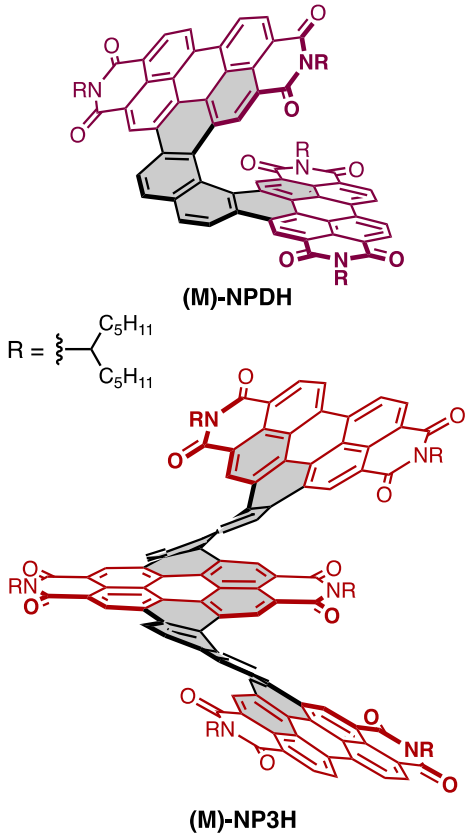

Figure 1. Chemical structures of (*M*)-**NPDH** and (*M*)-**NP3H** with subunits shown in red (PDIs) and black (naphthalenes). R alkyl group stands for 6-undecyl alkyl chains for both molecules, but they were replaced by methyl groups in the theoretical model. The aromatic rings composing the resulting carbo[6]helicene framework are highlighted in gray.

Extensive intramolecular overlap of the large PDI subunits ensures stability towards thermally-induced racemization, while the π-delocalization confers to these nanoribbons interesting electronic properties. In particular, these features impart the dense manifold of electronic states from 250 to 550 nm (5.0 to 2.2 eV) responsible for the remarkable absorption and ECD spectra. Here we show that time-dependent density functional theory calculations reproduce the experimental spectra, and we use several readily accessible computational tools to deconvolute the unexpected increase in ECD from **NPDH** to **NP3H**. Namely, we analyzed the difference of the electronic densities (DED) of the states that leads to the largest ECD response with respect to the ground state. The structural origin was further revealed by the calculations of different fragments within **NP3H** and the application of simple exciton

models on different fragments of the molecule. Importantly, we find that the naphthalene spacers together with a portion of the PDIs, which together constitute several idealized helicene subunits (i.e., carbo[6]helicenes, see colored rings in Figure 1), are the key to explaining the enhancement in ECD from **NPDH** to **NP3H**.

II. Computational details

Density functional theory (DFT) and its time-dependent (TD) extension for electronic excited states represent a good compromise between accuracy and computational cost; thus, they are usually the method of choice to investigate the optoelectronic properties of extended π-conjugated compounds, like conjugated polymers or nanoribbons.[17-22] We adopted the CAM-B3LYP functional to ensure a proper description of the excited states, including those with possible charge-transfer (CT) character.[23] Moreover, since the helical structure brings different parts of the molecule into close vicinity, the molecular geometry can be altered by non-covalent dispersion forces, with significant effects on the spectroscopic properties; therefore, we included Grimme's dispersion corrections with Becke-Johnson damping (GD3BJ).[24-26] Previous calculations of the ECD spectra of different functionalized helicenes have been reported in literature in the last decade, adopting TD-DFT (also in combinations with functionals with dispersion corrections) or even Coupled Cluster (CC2) methods.[7,27-32] Here, due to the necessity to perform an extended computational study, we used TD-DFT and moreover we mainly adopted the convenient 6-31G(d) basis set in the gas phase and replaced the 6-undecyl chains with methyl groups. The adequacy of this level of theory is carefully evaluated in the Supporting Information (SI). All calculations were performed with Gaussian 16 (see SI for more details),[33] except TD-DFT calculations of the rotatory strengths with the London Atomic Orbitals (LAO) that were performed with Dalton2016.[34]

The nature of the excited states was studied in terms of difference of electronic densities between the excited state *i* and ground state, and in the Supporting Information in terms of the Natural Transition Orbitals (NTOs).[35]

Absorption and ECD have been computed including the vibronic contributions at Franck-Condon (FC) with the Vertical Gradient (VG) harmonic model (FC|VG),[36] with the code FCclasses 3.0, considering the first 50 excited

electronic states for both **NPDH** and **NP3H**.[37] Vibronic calculations of the electronic spectra of helicenes were already reported but only for smaller systems and very few electronic states.[38,39]

In order to perform exciton ECD calculations, we defined suitable molecular models made up of different interacting species, and computed the couplings between their local excitations with Gaussian 16 as a Coulombic interaction of the transition densities. The ECD spectrum was then obtained with the program EXAT interfaced with Gaussian 16 (see Section S8 of SI for further details).[40]

III. Results and Discussion

III.A Reproducing the Experimental Spectra with TD-DFT

Figure 2 shows that our calculations in gas-phase reproduce the experimental spectral shapes in THF, apart from a slight overestimation of the intensity for **(*M*)-NP3H** and a moderate blue-shift (0.33 eV for **NPDH** and 0.39 eV for **NP3H**).. The simulated UV-vis spectrum of **NPDH** agrees with experiment nearly quantitatively from 550 up to 400 nm. In the same range, the general shape of its ECD, characterized by a negative band followed by two positive bands and a weak signal at higher energies, is also reproduced. For **NP3H**, the calculated and experimental UV-vis are almost identical for the first two lowest bands, while at λ of <450 nm we observed some underestimation of the relative intensity. The shape of the ECD spectrum of **(*M*)-NP3H** is nicely captured, with a negative band at ~510 nm and a very intense couplet at ~400 nm. In particular, the large enhancement of the chiroptical response at ~400 nm (the central point where the intensity is 0) of **(*M*)-NP3H** with respect to **(*M*)-NPDH** is consistent with our computations, although it is blue shifted to ~340 nm. For π-conjugated systems of this size, some discrepancies between computations and experiments should be expected, especially when high-energy states (shorter wavelengths) are considered. They can be due to several factors, including the coupling among the electronic states (e.g., for **NP3H**, there are 15 different electronic states from 300—370 nm, roughly corresponding to 360—430 nm in the experiment), whose proper inclusion is beyond the capabilities of state-of-the-art methodologies.

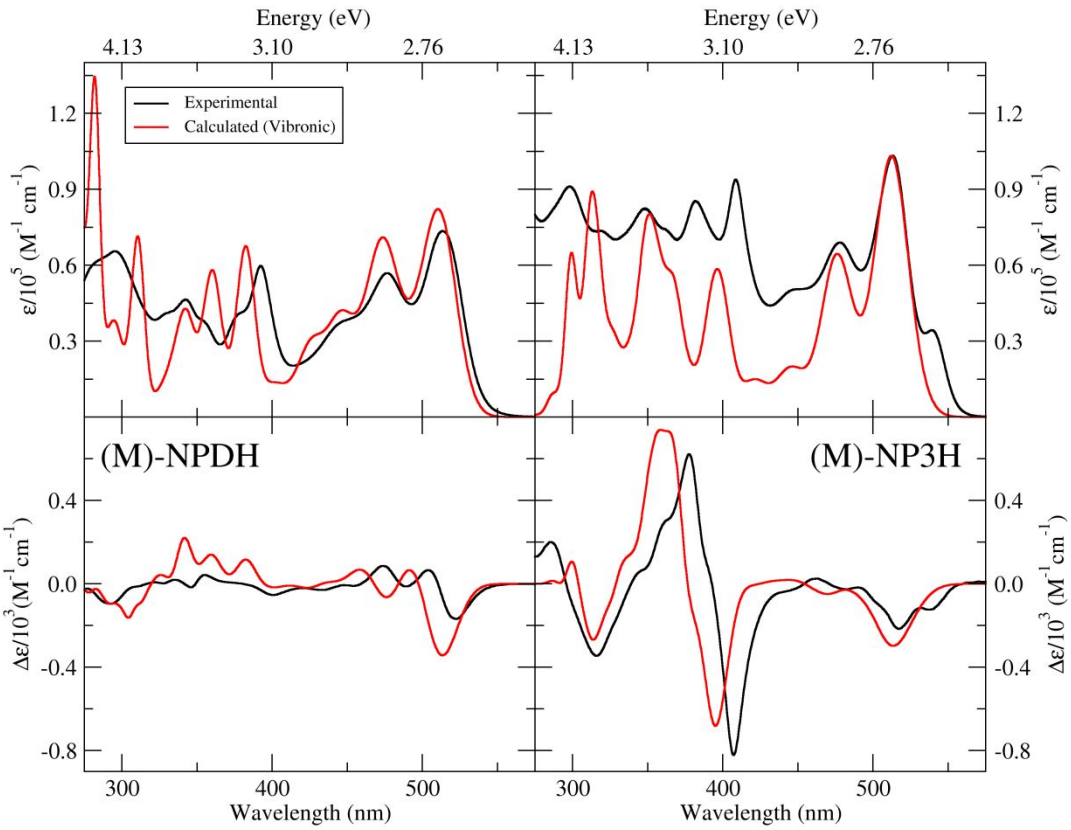

Figure 2. Comparison of computed (gas phase) and experimental (THF) absorption (top) and ECD (bottom) spectra of **(*M*)-NPDH** (left) and **(*M*)-NP3H** (right).[14,15] Calculated vibronic spectra (50 states) shown in red have been obtained with the FC|VG model and have been shifted by 0.330 eV for **(*M*)-NPDH** and 0.387 eV for **(*M*)-NP3H** to match the position of the long wavelength first peak. Additionally, the **(*M*)-NP3H** absorption and ECD intensities have been multiplied by a factor of 0.64; no scaling factor was needed for **(*M*)-NPDH**. Computed spectra have been convoluted with a phenomenological Gaussian with HWHM = 0.056 eV.

The good agreement of the computed vibronic absorption and ECD spectra with experiment prove that CAM-B3LYP/6-31G(d) level of theory is fully adequate to investigate the mechanism of the enhancement of the ECD activity in **(*M*)-NP3H**. Since the details of the vibronic shapes arise from the contributions of millions of different vibrational states, for further analysis we adopt a simpler purely-electronic approach, where vibronic contributions are neglected. In this approximation, the spectra are obtained simply from the transition frequencies of the electronic excited states and their intensities, each of which is associated with a Gaussian linewidth. **Figure 3** shows that such

a simplified model still captures the main features of the spectra and, in particular, it describes the ECD enhancement of **(*M*)-NP3H** observed in the experiments very well. Yet, some changes are evident: for example, the relative intensity of the second band in the absorption spectrum of **NPDH** and **NP3H** at 475 nm is reproduced at the vibronic level but is remarkably underestimated by the pure electronic approach. Moreover, the lowest energy absorption band (~500 nm) is overestimated by a purely-electronic calculation, because the intensity is concentrated in a single band and not distributed on the different vibronic peaks.

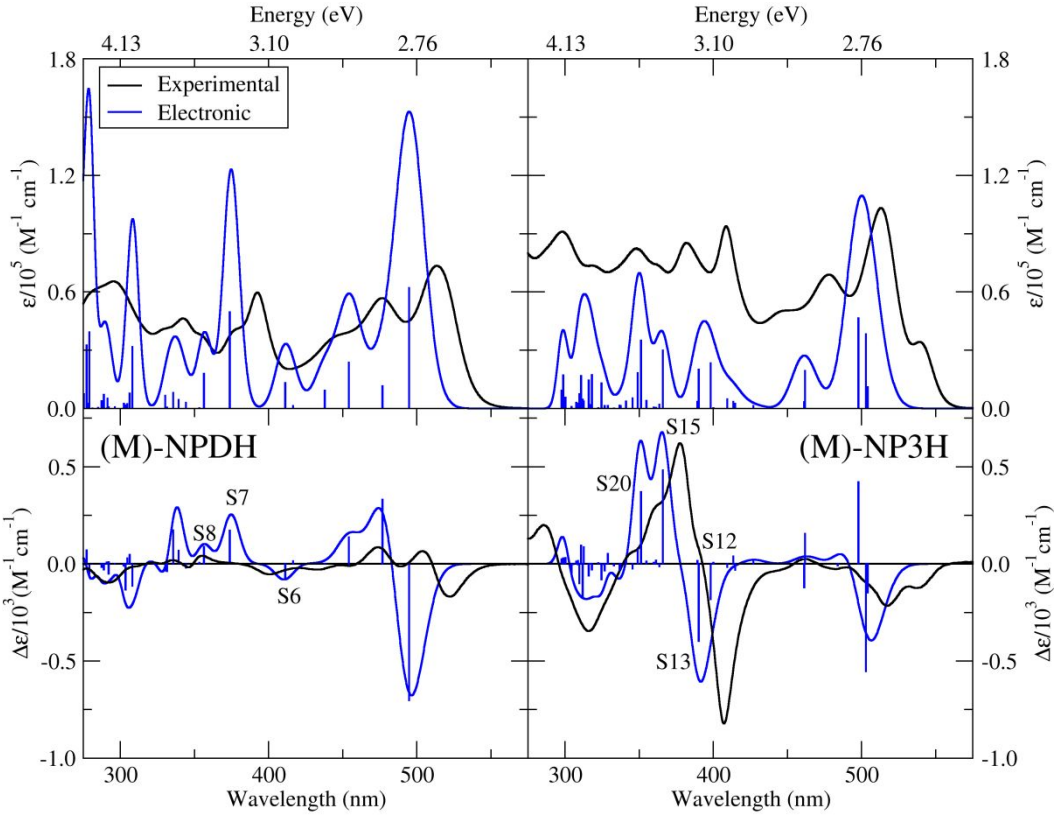

Figure 3. **(*M*)-NPDH** (left) and **(*M*)-NP3H** (right) absorption (top) and ECD (bottom) spectra computed at the pure electronic level and stick bands for the individual states. We label the most important states (in order of increasing energy). All stick electronic bands have been convoluted with a phenomenological Gaussian with HWHM = 0.056 eV. A red-shift on the energy axis of 0.330 eV for **(*M*)-NPDH** and 0.387 eV for **(*M*)-NP3H** has been applied. The **(*M*)-NP3H** absorption and ECD intensities have been multiplied by a factor of 0.64. These shifts and scaling are the same values adopted for the vibronic spectra in **Figure 2.**

As mentioned above, the absolute position of the computed spectra is moderately blue-shifted (~0.33 eV for **(*M*)-NPDH** and ~0.39 for **(*M*)-NP3H**), in line with what is expected for CAM-B3LYP.[41] In the SI (Section S1), we show that the inclusion of solvent effects with the polarizable continuum model (PCM)[42] and the usage of larger basis sets partially reduce this error (to ~0.16 eV and ~0.22 eV for **(*M*)-NPDH** and **(*M*)-NP3H,** respectively), but they do not significantly change the spectral shapes; therefore, the level of theory adopted is adequate for the forthcoming analysis. The experimental absorption spectrum of **NP3H** shows a low-energy shoulder (~540 nm) that is apparently missing in our computations. This issue is analyzed in Section S2 of the SI. There, we show that this shoulder likely arises from the S1 state, which is too close to the other states in our computations.

In the region of the ECD couplet (~340 nm for computed values), **NPDH** and, most of all, **NP3H** exhibits several electronic states (namely, 15 states within 0.6 eV for **NP3H**). Notwithstanding this, the main contributions to the ECD arise from only a few states, whose properties are reported in **Table 1**. In particular, in the region of interest, three states mainly contribute to the ECD of **(*M*)-NPDH**: S6 (negative), S7 (positive) and S8 (positive); and four states are important for the ECD of **(*M*)-NP3H**: S12 and S13 (negative) and S15 and S20 (positive).

Table 1. Vertical excitation (VE) in eV, its corresponding λ (nm), oscillator strength (OS), rotatory strengths (all in 10^{-40} cgs units) in the velocity gauge (R_{vel}) and in the length gauge R_{LAO}(with London atomic orbitals (LAO) module of the electric (**μ**) in a.u., and m_μ (the component of the imaginary part of the magnetic transition dipole moment, **m,** along **μ**, also in a.u.) for the excited states involved in the largest ECD activity of **(*M*)-NPDH** and **(*M*)-NP3H**. Calculations at CAM-B3LYP/6-31G(d)/GD3BJ level of theory in gas phase with R = Me.

(*M*)-NPDH							
Excited State	VE	λ	OS	R_{vel}	R_{LAO}	**μ** module	m_μ (LAO)
S6	3.35	370	0.13	-79	-77	1.28	-0.13
S7	3.65	340	0.50	167	187	2.36	0.16
S8	3.81	325	0.18	85	94	1.39	0.14
(*M*)-NP3H							
Excited State	VE	λ	OS	R_{vel}	R_{LAO}	**μ** module	m_μ (LAO)
S12	3.50	354	0.28	-451	-461	1.81	-0.55
S13	3.57	348	0.24	-953	-945	1.67	-1.36
S15	3.78	328	0.36	1146	1147	1.97	1.30
S20	3.92	316	0.42	911	916	2.09	0.93

Origin-independent calculations of the rotatory strength (RS) of an electronic state can be obtained in the velocity gauge (R_{vel}) and in the length gauge adopting London atomic orbitals (R_{LAO}), while using conventional orbitals, origin-invariance is only assured for exact wavefunctions and infinite basis sets.[43] In order to analyze in deeper detail differences between **(*M*)-NPDH** and **(*M*)-NP3H**, we consider that fact that RS in the length gauge is the scalar product of the electric ($\boldsymbol{\mu}$) and magnetic (**m**) transition dipole moments and, since **m** is not origin-invariant in the following we focus our analysis on $\boldsymbol{\mu}$ and on m_{μ}, the component of **m** along $\boldsymbol{\mu}$ (i.e. the only one relevant for the RS).[43] Data in **Table 1** show that while the magnitude of $\boldsymbol{\mu}$ slightly changes from **(*M*)-NPDH** to **(*M*)-NP3H**, all the states involved in **(*M*)-NP3H** couplet exhibit a very large enhancement of m_{μ}, by a factor ranging from 3.5 to 9 (considering states with same sign of the RS). This phenomenon accounts for most of the 15-fold enhancement of the ECD response of **(*M*)-NP3H** with respect to **(*M*)-NPDH** observed in the experiment at ~400 nm. Further minor contributions to the positive part of the couplet in the **(*M*)-NP3H** arise from other excited states (see stick lines on Figure 2). More precisely, the inclusion of all the states contributing to that spectral region results in an enhancement factor for the total rotatory strength of 13.3 times with respect to **NPDH**, while the sum of the contributions of S15 and S20 provided an enhancement of 12.3.

Section S3 in the SI shows that as far as the analysis of m_{μ} is concerned, very similar results can be obtained also using convential orbitals, both placing the origin in the center of mass and displacing it. Moreover, the conclusions of our analysis are confirmed even adopting the much larger basis set 6-311+G(2d,2p). Alternative strategies to face with the problem of origin dependence were introduced in ref. 32.

In summary, the reproduction of the absorbance and ECD spectral profiles and of the enhancement in molar ECD for **NP3H** strengthens the validity of the underlying calculated electronic structures of **NPDH** and **NP3H**. It also allows us to *quantitatively* rationalize most of the enhancement of the ECD of **(*M*)-NP3H** as an increase of the magnetic transition dipoles of a few relevant excited states. In the following section the properties of such electronic states will be further analyzed to draw a *qualitative* rationale for the ECD enhancement.

III.B A Qualitative Understanding of the Mechanism of ECD Enhancement

III.B.1 Analysis of the relevant states

The most straigthforward description of TD-DFT electronic states is the excitations between Kohn-Sham (KS) molecular orbitals (MOs). For the states in **Table 1**, such analysis is not effective because the involved MOs are numerous and, in general, spread over the whole molecule (see SI Section S4, Figures S6—S10). Additionally, at least for **NP3H**, these states arise from several different transitions with comparable weights (and involving different MOs), so that for many states the largest contribution is only 30% of the total weight.

Therefore, we resorted to two alternative approaches: analysing the relevant excited states either in terms of the difference of their electronic densities (DED) with respect to the ground state, or in terms of NTOs. DED allows us to identify which parts of the molecule are more involved in the electronic transition (i.e., to monitor where the electronic density changes as a consequence of the excitation). On the other side, NTOs furnish a reading of the states in terms of transitions between MOs, which is simpler than using canonical (KS) MOs. The two approaches provide a convergent picture, but here we only focus on DED, while the NTOs are analyzed in Section S5 of the SI. The plots of DED are two-color surfaces: red indicates a density increase (where the electron is going upon the transition) and blue a density depletion (where the electron is moving from and, therefore, where a hole is formed). **Figures 4** and **5** show, respectively, the DED for **(*M*)-NPDH** and **(*M*)-NP3H** states (additional vantages are available in Section S6, Figure S27, and animations are reported as additional supporting information).

We first focus on the simpler **(*M*)-NPDH**. S6 is mainly a local excitation of the cores of the PDIs; in contrast (and very interestingly), S7 (the one carrying the largest RS in the analyzed energy region) only involves the central carbo[6]helicene, i.e., the napthalene moiety and the adjacent fused rings. Finally, S8 involves both the naphthalene and PDIs, exhibiting some CT character from the the central carbo[6]helicene to the outer parts of the PDIs. The situation is very different for **(*M*)-NP3H**: for S12 (negative), S15 (strongest positive) and S20 (positive), the DED is almost exclusively localized on the two carbo[6]helicene moieties. In S13, which carries the strongest negative RS, the DED involves the two carbo[6]helicenes but also evidences some CT contribution from the central PDI to the external PDIs. This contribution should not be important for the rotatory strength. In fact, we recall that if the involved orbitals are well separated and do not overlap CT transitions have a vanishing electric transtion dipole; therefore

they do not exhibit absorption and ECD signals. We emphasize that the DED plots on the two carbo[6]helicenes are very similar for S12, S13 and S20. They also resemble the DED plot of the carbo[6]helicene of **(*M*)-NPDH** for the S7 state. This resemblence can be better appreciated by focusing on the color pattern of the lobes, which we label with lower-case letters. In particular, note the large hole density (blue) on the naphthalene central bond (labeled as "e"), as well as the same alternating sign pattern on the carbo[6]helicene fragments (check lowercase letters a-i in Figures 4 and 5). S15 also exhibits a similar pattern of lobe signs, although with some differences.

This analysis shows that at least a significant part of the ECD enhancement in **(*M*)-NP3H** derives from states localized on the carbo[6]helicene subunits. However, carbo[6]helicene alone shows a much smaller ECD intensity in this energy region[Error! Bookmark not defined.] (see computed spectrum in Figure S28 of the SI); therefore, the origin of the enhancement in **(*M*)-NP3H** is due to the coupling between the states on the two carbo[6]helicenes. Although these two moieties are in principle π-conjugated in **(*M*)-NP3H**, their interaction resembles an exciton mechanism: (a) In exciton dimers arranged in a chiral geometry, large ECD arises because each monomer (in our case the carbo[6]helicene) acquires an additional apparent magnetic transition dipole (Section S8 of the SI).[18] As shown above, large magnetic transition dipoles (**Table 1**) account quantitatively for the enhancement in ECD of **(*M*)-NP3H**. Moreover, (b) an ideal symmetric exciton dimer would exhibit two eigenstates, splitted in energy, that are exactly the symmetric and anti-symmetric combinations of the same localized states on the monomers, and therefore, have identical DED. S12 and S20 states of **(*M*)-NP3H** have indeed identical DED on the carbo[6]helicenes moieties. Certainly, since **NP3H** is π-conjugated and exhibits a dense manifold of quasi-degenerate electronic states, these exciton-like states actually couple to other close-lying states. As a consequence, in **(*M*)-NP3H**, 4 (not simply 2) states are relevant for the largest ECD couplet, a very similar DED is observed also for S15, and some CT character also arises for states S12 and S13, which remarkably complicates our analysis.

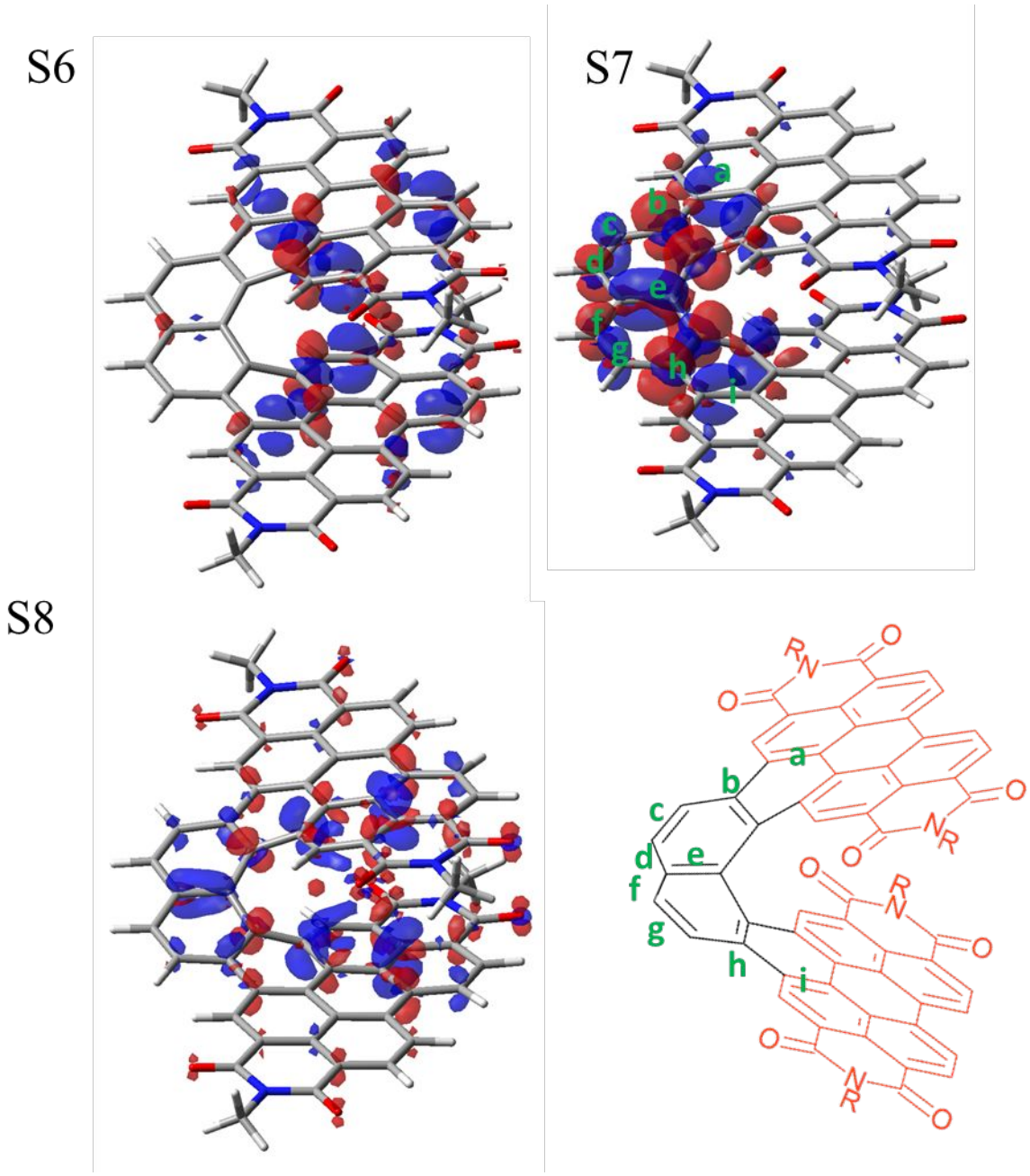

Figure 4. Difference of electronic density with respect to the ground state for S6, S7 and S8 singlet excited states of (*M*)-**NPDH** at the CAM-B3LYP/6-31G(d)/GD3BJ level of theory in the gas phase with R = Me. Isovalue = 0.001 electrons/bohr^3. The red and blue lobes correspond to an increase and decrease in electron density, respectively. We labeled the rings and relevant lobes of S7 with lower-case letters (from a to i) to better compare its DED to the plots of **NP3H** (Figure 5). For reference (and to highlight the naphthalene and PDI fragments), the structure of (*M*)-**NPDH** is also shown (right-bottom corner) in the same orientation as the density plots. The position of the most relevant lobe labels of S7 have also been included in this structure.

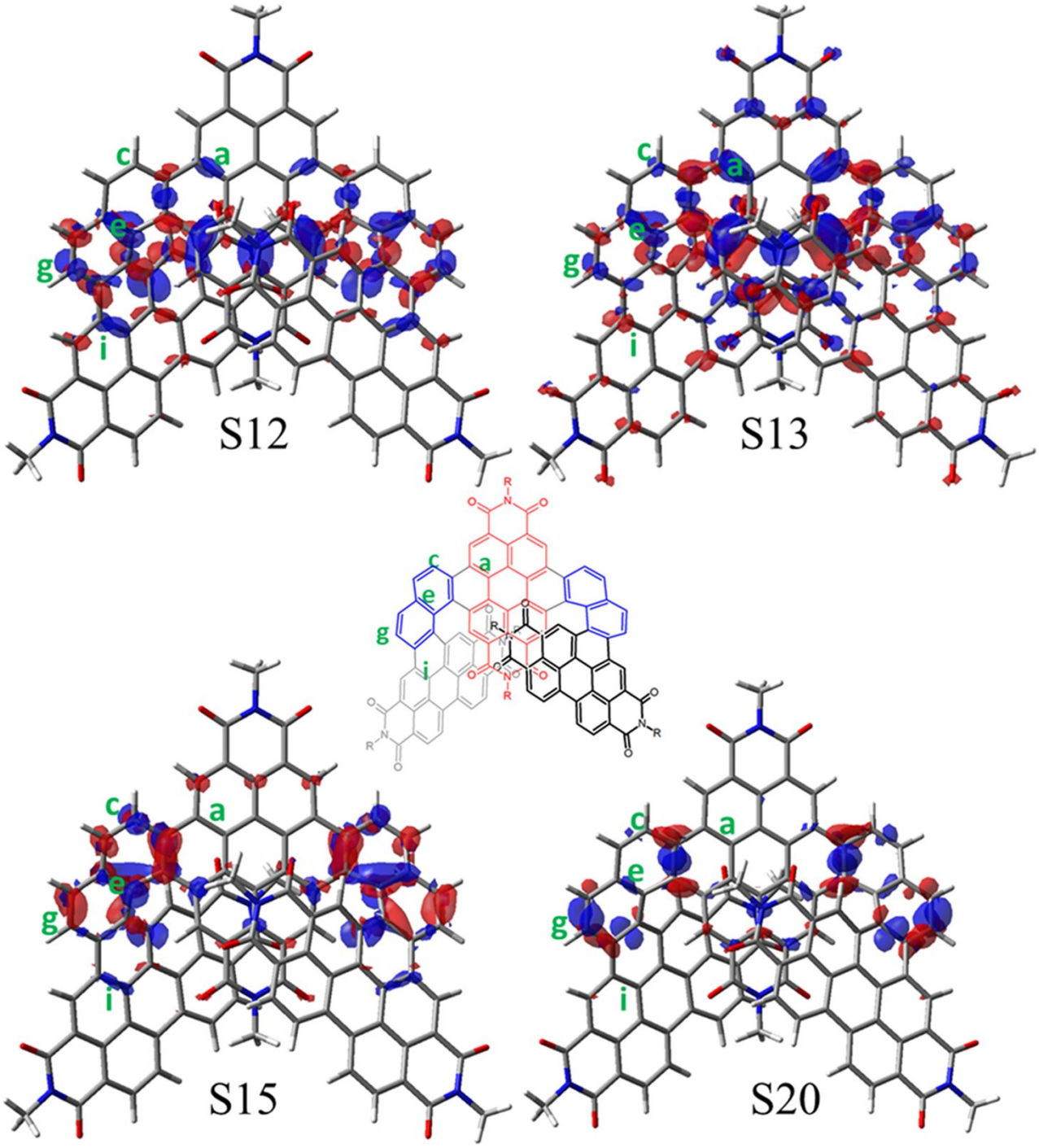

Figure 5. Difference of electronic density with respect to ground state for S12, S13, S15, and S20 excited states of (*M*)-**NP3H** at the CAM-B3LYP/6-31G(d)/GD3BJ level of theory in the gas phase with R = Me. Isovalue = 0.0008 electrons/bohr^3 . The red and blue lobes correspond to an increase and decrease in electron density, respectively. For reference (and to highlight the naphthalene fragments), the structure of (*M*)-**NP3H** is also shown (center) in the same orientation as the density plots. The position of the most relevant lobe labels have also been included in this structure.

An exciton-like coupling between states localized mainly on the carbo[6]helicenes moieties can, clearly, only be operative for **NP3H** (and longer members of the series **NP*n*H**, where *n* denotes the number of PDI subunits), since they incorporate two or more carbo[6]helicenes within their frameworks; **NPDH** incorporates just one. Therefore, an exciton-like mechanism between idealized carbo[6]helicenes provides a simple explanation of the strong enhancement in ECD of **(*M*)-NP3H** with respect to **(*M*)-NPDH.**

III.B.2 TD-DFT Computations on fragments of (*M*)-NP3H

We reinforce the conclusion about the central role of carbo-helicenes and of exciton-like interactions by calculating the ECD of model systems, in which we artificially removed parts of the original **(*M*)-NP3H** molecule (see Figure 6) and/or break the π-conjugation.

Fragment 1 is a simplified structure of **(*M*)-NP3H,** where only two helicene moieties and the minimal number of atoms to connect them were conserved. Notice that **Fragment 1** incorporates two carbo[5]helicenes, i.e., one ring of each carbo[6]helicene in the parent **(*M*)-NP3H** is lost. The advantage of this structure is that it allows us to very easily study the effect of the conjugation by simply saturating the two carbons of the central aromatic ring. In this way, we obtain **Fragment 2**.

We computed the ECD for **Fragment 1** and **Fragment 2**, both frozen in the **(*M*)-NP3H** arrangement, i.e., without reoptimizing their structures (Figure 6). In the same region of the strongest ECD of **(*M*)-NP3H** (~340 nm, computed values), **Fragment 1** exhibits a comparably strong ECD couplet (although red-shifted by ~30 nm). This finding indicates that only small portions of the PDI subunits are involved in the enhancement of ECD in **(*M*)-NP3H**. We also notice that: (a) the ECD of **Fragment 1** is much larger than the one predicted for carbo[5]helicene (Figure 6); and (b) **Fragment 2**, obtained from **Fragment 1** by breaking the π-conjugation between the helicene subunits, shows even larger ECD. The strong ECD of **Fragment 2** proves that the π-conjugation between the two carbo[5]helicenes is not essential for the enhancement of the chiroptical response with respect to the carbo[5]helicene monomer. We also studied an alternative model system (**PDI_3**) consisting of three PDI molecules constrained to the same position

that they occupy in **(*M*)-NP3H**. **PDI_3** is predicted to have only a very weak ECD response at λ < 430 nm (Figure 6). Although it should be recalled that chiroptical properties are not additive and therefore a comparison of the ECD of a molecule and some of its fragments must be done with caution, this result underscores the limited contribution of the PDI subunits to the strong ECD in NP3H at 400 nm (340 nm in the computation), in the sense that it shows that the three units of PDI alone cannot explain such ECD if the role of the conjugated NPs is neglected.

The above findings clearly support that the strongest ECD couplet in **(*M*)-NP3H** is largely due to an exciton-like coupling between states localized on the carbohelicene branches, i.e., on the substructures made up by the naphthalenes plus the adjacent fused rings of the PDIs. Still, it is important to clarify that the role of the perylenes is not entirely negligible, which will be discussed in more detail in the following section. We also emphasize that, according to calculations, **PDI_3** does feature a large ECD couplet, but this couplet is located in the 450—500 nm region. The same region for **(*M*)-NP3H** shows only a moderately intense negative band; therefore, the **(*M*)-NP3H** structure actually suppresses partially the ECD activity that could potentially arise from its PDI subunits.

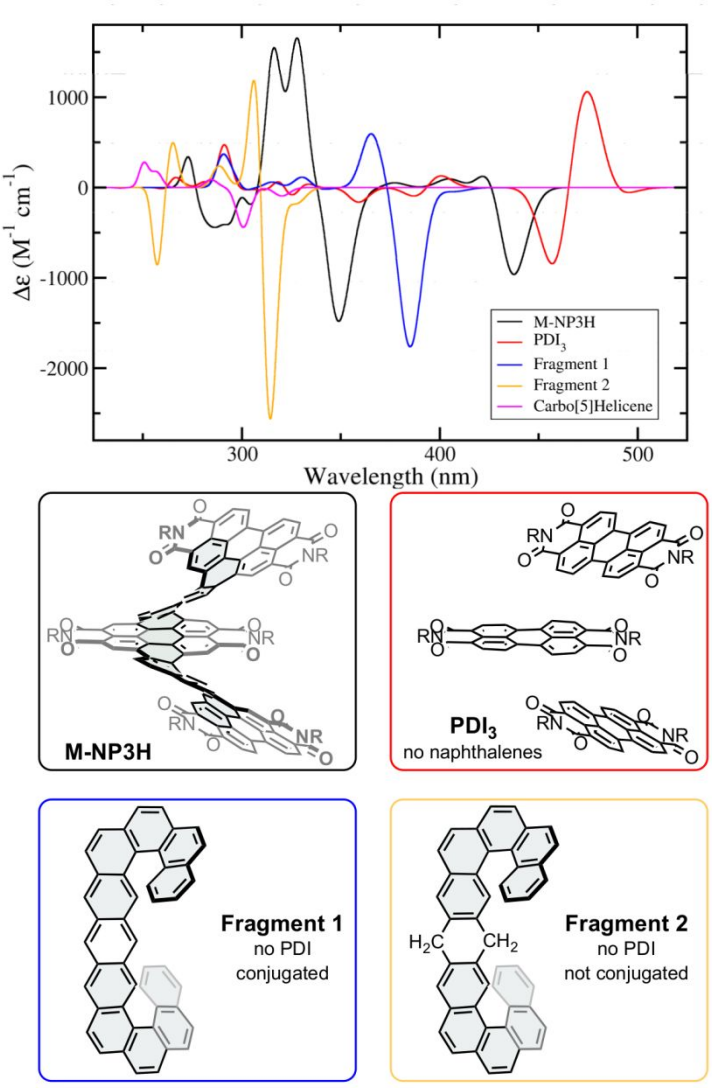

Figure 6. Comparison of the ECD computed for **(*M*)-NP3H** and for model systems corresponding to fragments of **(*M*)-NP3H. Fragment 1** and **Fragment 2** were obtained from the portion of the **(*M*)-NP3H** structure highlighted in gray. Saturating the central ring of **Fragment 1** interrupts the conjugation between its two carbo[5]helicene subunits, giving **Fragment 2**. We generated **PDI_3** from **(*M*)-NP3H** by simply retaining the PDI subunits. All fragments were constrained to the geometry that they adopt in **(*M*)-NP3H**, and dangling bonds were saturated with hydrogens. The calculated ECD spectrum of (*M*)-carbo[5]helicene is also displayed.

III.B.3 Exciton model calculations

In order to finally prove that an exciton mechanism between the carbohelicenes subunits can be responsible for the strong ECD observed in **(*M*)-NP3H**, we now build a truly excitonic dimer, **[5]Hel dimer,** made up by two carbo[5]helicenes frozen in the position they have in **(*M*)-NP3H**. The model, illustrated in Figure 7, can also be considered like an exciton model of **Fragment 2**. Like for **Fragment 2, [5]Hel dimer** incorporates carbo[5]helicenes and not carbo[6]helicenes, since the latter would share two carbon atoms (see Figure 1).

Figure 7 shows that the ECD of **[5]Hel dimer** computed with an excitonic model is comparable with the ECD of **(*M*)-NP3H** and **Fragment 2** computed with TD-DFT. Notice that the RS (stick lines) for the exciton model are predicted to be as large as those computed with TD-DFT for **Fragment 2** and even larger than those of **(*M*)-NP3H**. However, the splitting between the excited states carrying a positive and a negative RS in **[5]Hel dimer** is smaller than for **Fragment 2** and much smaller than for **(*M*)-NP3H** . As a consequence, the positive and negative bands partially cancel, resulting in narrower and less intense ECD couplets.

As far as the position of the bands is concerned, for **[5]Hel dimer** they fall at shorter λ, with a difference that is particularly significant with respect to the negative bands of **(*M*)-NP3H.** This difference evidences that the missing parts of the chemical structure of **(*M*)-NP3H** do affect the properties of the electronic states responsible for the strongest ECD bands. It is worthy to clarify that **[5]Hel dimer** was not designed to be a full-model of **(*M*)-NP3H** (some parts of the molecular are clearly missing) but to show that the exciton coupling between the two **[5]Hel** held in the position they have in **(*M*)-NP3H** gives rise to a very strong ECD couplet, qualitative similar to the one observed for **(*M*)-NP3H**. Of course, different exciton models could be imagined. Figure S31 in the SI reports the computed ECD for alternative excitonic systems, and namely a dimer in which each **[5]Hel** is bound to the external PDIs (**[5]Hel-PDI dimer)** or a **5-units model** comprising the 3 PDIs and 2 NPs. They provide consistent predictions for the strong ECD couplet, further enforcing our conclusions. Of course, according to the **5-units model,** the strong couplet is remarkably blue-shifted because it arises essentially from the interaction of electronic states of the shorter NPs moieties. Beside this, results in the SI show that different molecular models (most of all if several electronic states are considered for each fragment) can also lead to the prediction of additional bands which do not have a clear counterpart in (*M*)-NP3H. This is of course not strange, but it helps us to stress that in systems like **(*M*)-NP3H**

which exhibit a π-conjugation, in principle extending over all the molecular structure, the exciton-like picture remains an approximation. Therefore, while we showed that exciton models are useful to analyze the origin of a specific property like the strong ECD couplet at 400 nm, they cannot of course be used as a black-box to compute all the properties of NPnH systems.

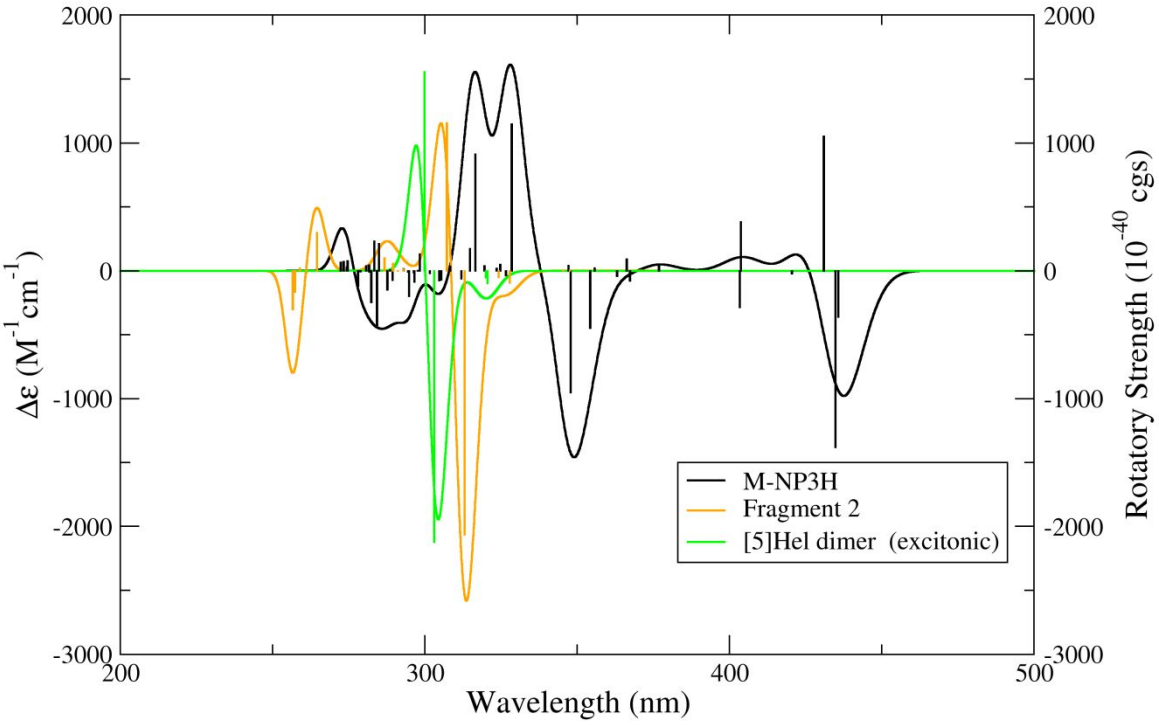

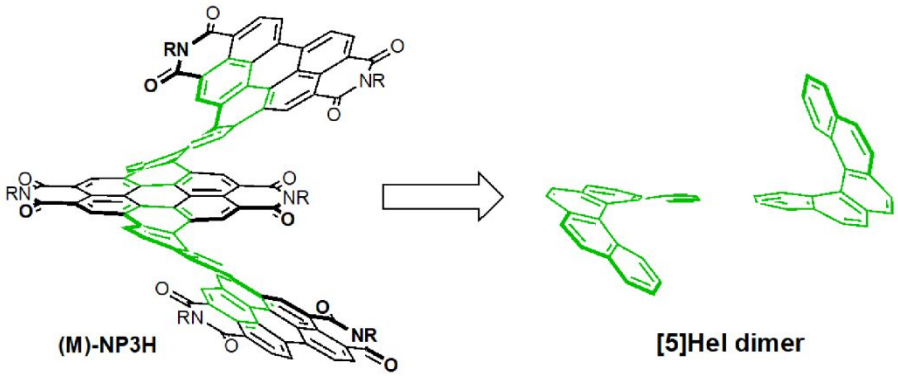

Figure 7. Comparison of the ECD for (*M*)-**NP3H** and the model **Fragment 2** computed at the TD-DFT level, and the spectrum of **[5]Hel dimer** computed by an excitonic model. All stick electronic bands have been convoluted with a phenomenological Gaussian with HWHM = 0.056 eV

It is now interesting to inquire if this exciton-like picture is also able to explain the change in the ECD response for at least mild changes in the molecular structure. As discussed in Section S1, we optimized (*M*)-**NP3H** with two different procedures, i.e. including or not dispersion corrections (GD3BJ). Figure 8 shows that the ECD shapes predicted for the two structures are similar, but the intensity of the structure optimized without dispersion corrections is higher. Since, as shown in the inset of Figure 8, the structure optimized without GD3BJ is more stretched ("Elongated") along the helical axis than the structure obtained with GD3BJ ("Compact"), this finding suggests a correlation between the extension along the helical axis and the intensity of the ECD signal.

Figure 8 shows that the simple exciton model reproduces this trend. More in detail, we adopted the exciton approximation to compute the spectra of **[5]Hel dimer** also in a geometry corresponding to the Elongated structure of (*M*)-**NP3H**. In this way we managed to reproduce the ECD couplet of the Elongated structure and the fact that is more intense (and slightly blue-shifted) with respect to the spectrum of the Compact structure. Further details are given in the SI.

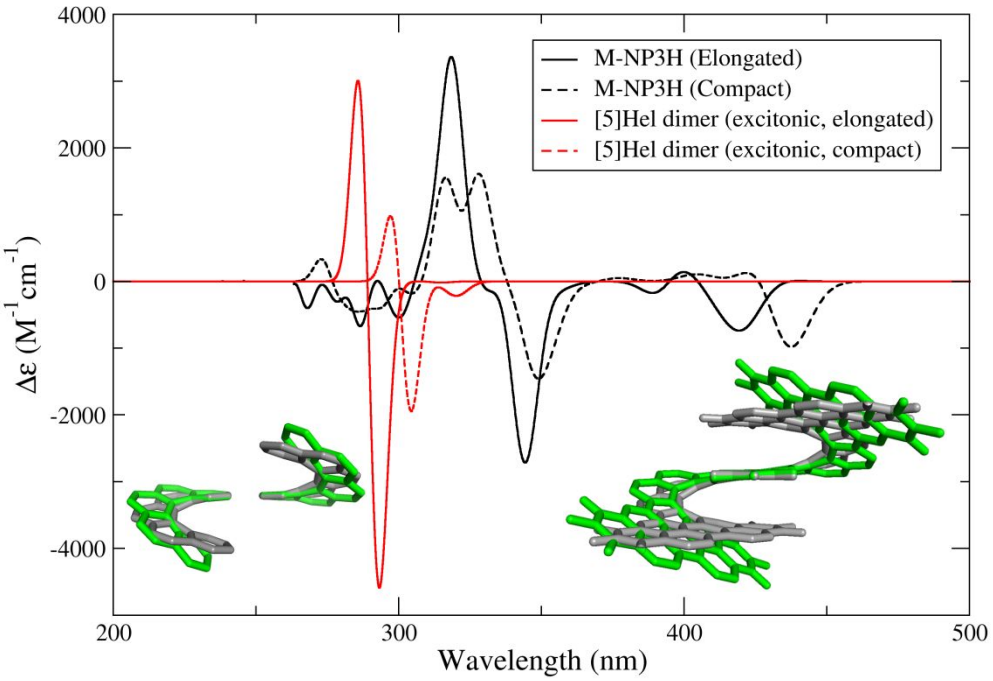

Figure 8. Comparison of the ECD spectra of **(*M*)-NP3H** in the structures optimized without GD3BJ corrections (Elongated, green structure) and with GD3BJ corrections (Compact, gray structure) with the ECD spectra for the corresponding structures of **[5]Hel dimer** obtained by applying the exciton model. All stick electronic bands have been convoluted with a phenomenological Gaussian with HWHM=0.056 eV. The superposition of structures was realized with PyMOL software[44] and the hydrogen atoms were hidden for clarity.

To summarize, the enhancement of the ECD intensity of **(*M*)-NP3H** at 400 nm quantitatively arises from a large increase of the transition magnetic dipole moments of a few selected states (Table 1). This phenomenon can be qualitatively understood by considering the carbo[6]helicenes as key chromophores (formed by the naphthalenes and the adjacent fused rings of the PDI) that interact through an exciton-like coupling. Such an exciton-like mechanism is also able to reproduce the variations of the ECD predicted by TD-DFT with the axial elongation of the molecular structure. It is, however, important to highlight that this picture is only qualitative; in reality, all of the aromatic subunits in (***M***)-**NP3H** exhibit some degree of π-conjugation. In addition, the role of the PDI subunits is not negligible. First, they provide the fused rings to form these “idealized” carbo[6]helicenes chromophores. Second, the electronic states responsible for the strongest ECD couplet in (***M***)-**NP3H** (and mainly attributed to the

carbo[6]helicenes) would clearly be different without the PDIs: in the experimental spectrum, these states absorb in the visible, rather than in the UV region like for the isolated carbo[6]helicene.

PDIs clearly have "electronic" effects, due to the π-conjugation, on the electronic states responsible for the most intense ECD of **NP3H**. For instance, it is quite evident in Figure 5 that the DED of state S13 also involves the central PDI. Moreover, even focusing on the carbohelicene subunits, we notice that the DED of the strongest ECD states of **(*M*)-NP3H** resemble, but do not coincide, with those expected for any electronic state of the isolated carbo[6]helicene (see SI, Section S5). Third, the conjugation between these idealized carbohelicenes, induced by the PDI, increases their couplings and, therefore, their splitting, thus avoiding mutual cancellations of the positive/negative peaks (which occur in the simple exciton model in Figure 7). Such an effect of the conjugation between the two carbohelicenes can also be deduced by the larger splitting of the ECD peaks of **Fragment 1** (conjugated) with respect to **Fragment 2** (non-conjugated) in Figure 6.

PDIs also play a relevant "structural" role, besides preventing the thermally-induced inversion of the helix: they dictate the mutual orientation of the carbo[6]helicenes, and the exciton-model in Figure 7 shows that such orientations correspond to strong ECD bands. Other double- or multibranch-helicenes show only moderate enhancement or even a quenching of the ECD signal with respect to the carbo[6]helicene.[45] Also, we can deduce that the structural constraints due to PDIs partially contribute to the observed red-shift of the ECD couplet, which moves from the UV (carbo[4]-, carbo[5]-, carbo[6]-helicenes) to the visible in **(*M*)-NP3H**. This phenomenon is illustrated by further consideration of **Fragment 1** and **Fragment 2**. Specifically, releasing the constraints imposed by the scaffold of **(*M*)-NP3H** and re-optimizing the structures of **Fragment 1** and **Fragment 2** elicits large blue-shifts in their strong ECD couplet: namely ~45 nm for **Fragment 1** and ~22 nm for **Fragment 2** (see Figure S29 of the SI). This effect can be observed already for the simple carbo[6]helicene units in **(*M*)-NP3H**. Optimization of their structure, in fact, leads to a blue-shift of the ECD by ~27 nm (Figure S28). Interestingly, the blue-shift predicted by TD-DFT for the optimized structure of **Fragment 2** is also reproduced by an excitonic calculation on **[5]Hel dimer** (Figure S33 of the SI).

III.C Double[6]Helicene

We can reinforce the conclusions we reached by considering hexaheliceno[3,4-*c*]hexahelicene, a double[6]helicene synthesized in 1972 but for which ECD has never been reported.[46] In fact, this double[6]helicene can be thought as a different fragment of **(*M*)-NP3H**. Conformational analysis shows that it can adopt two different conformations for the central cove, (*P*) or (*M*). Considering internal energy only at CAM-B3LYP/6-31G(d) in the gas phase, the left cove is predicted to be more stable by 5.5 kcal/mol and, therefore, dominant at room temperature. Still, an accurate study of the relative stability is not essential: both conformers exhibit similar ECD spectra, which we compare to the ECD of **(*M*)-NP3H** in Figure 9. They exhibit spectra similar in intensity and shape to the spectrum of **(*M*)-NP3H** (notwithstanding the blue-shift of ~30 nm). A similar ECD spectrum is also predicted for a closely related compound with a flat cove in which a methylenic unit is placed on the central aryl ring. The comparison of this compound with carbo[6]helicene evidences a significant enhancement of the intensity by a factor of <2 for the negative band and a factor of >4 for the positive band, together with a red-shift by ~30 nm. Figure S30 in the SI shows that the structure of the flat cove of this double[6]helicene is more similar to the Elongated than to the Compact structures of **(*M*)-NP3H**, while the predicted maximum intensity of the ECD couplet is intermediate between the two (compare also Figure 8 and 9). The difference between the ECD of the double[6]helicene and the two structures of **(*M*)-NP3H** confirm that, of course, the effect on the strongest ECD couplet of the **(*M*)-NP3H** rings not included in the double[6]helicene is not completely negligible.

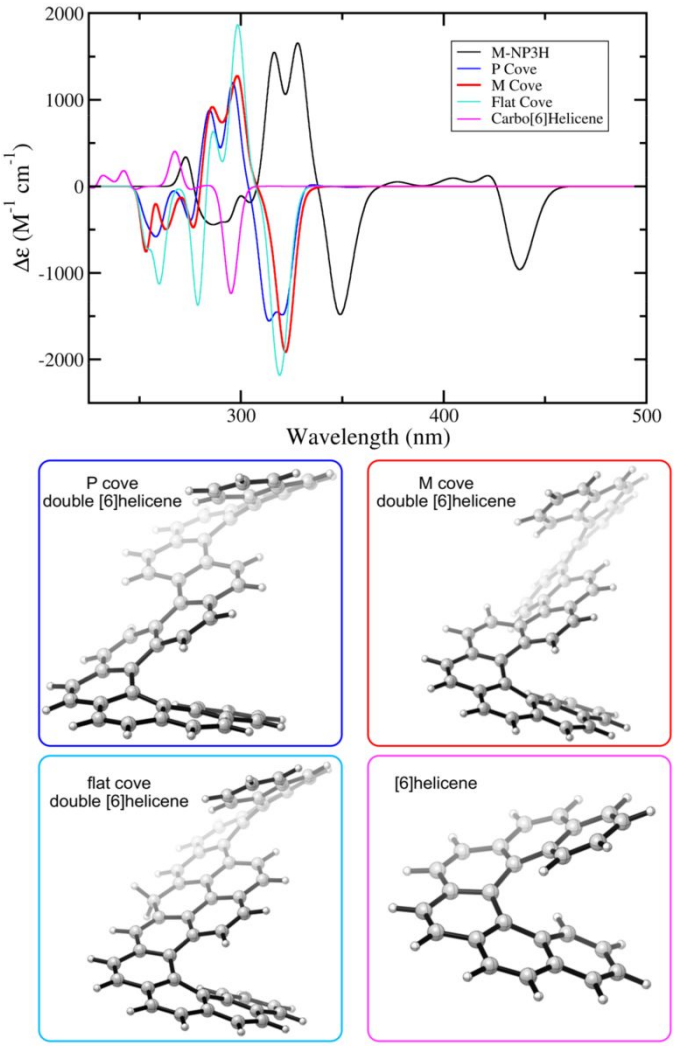

Figure 9. Comparison of the ECD spectra predicted at TD-DFT (CAM-B3LYP/6-31G(d)/GD3BJ) for **(*M*)-NP3H,** the two conformers of the double[6]helicene (*P* cove and *M* cove), the flat cove and [6]helicene.

IV. Summary and Conclusions

In this work we adopted TD-DFT and a number of interpretative tools of computational chemistry to investigate the origin of the ECD amplification from **NPDH** to **NP3H.** We found that it arises from an increase of the magnetic transition dipole on states that are mainly localized on its carbo[6]helicenes subunits. Fragment analysis confirms that the PDI units alone cannot explain the enhancement, which, on the contrary, exists also for simple

double[6]helicene structures. The amplification in **NP3H** with respect to **NPDH** originates from an exciton-like interaction between its two carbo[6]helicenes units. The same amplification could, therefore, be observed in related multi-helicene systems. In particular, double[n]helicene configurations analogous to the double[6]helicene subunit in **NP3H** can be responsible for the large ECD in other systems as well, and, therefore, it could serve as a model for the design of excellent chiroptical materials.**Error! Bookmark not defined.** In 1972, the hexaheliceno[3,4-*c*]hexahelicene, a double[6]helicene, was synthesized but its ECD has never been reported.[46] We predict also for this molecule a strong ECD couplet at wavelengths similar to **(*M*)-NP3H** As a matter of fact, this particular double[n]helicene configuration was found to be effective for enhancing chiroptical properties in other examples as well.[47] Furthermore, the existence of an exciton-like mechanism in **(*M*)-NP3H** makes understandable why additional ECD amplification has been observed when more pairs of symmetrically equivalent helicenes are incorporated into these frameworks.[48]

The capability of TD-DFT calculations in combination with CAM-B3LYP to reproduce the experimental ECD spectra and, in particular, the amplification from **NPDH** and **NP3H** can also assist the search and the design of alternative nanoribbons with outstanding chiroptic properties. On the other side, our results show that, at the increase of the size and the electron delocalization, computations become more and more expensive and their interpretation complex. As such, the qualitative understanding of the amplification mechanism with simple exciton models could turn useful for further developments. In the future it will be interesting to inquire the potentiality of a multi-step protocol to facilitate the discovery of helicene-based new chiroptical materials: one can first exploit exciton models for a qualitative large exploration of possible helicenes, investigating not only the impact of the chemical nature of the subunits of the nanoribbons but also, in an extensive manner, their best mutual arrangement; afterward one can use this information to design candidates with a viable synthetic route and check their properties with more accurate TD-DFT calculations.

Supporting Information

The Supporting Information is available free of charge at https://pubs.acs.org/.

Further computational details. Analysis of the lowest absorption band in **(*M*)-NP3H**. Analysis of the relevant Kohn-Sham and Natural Transition Orbitals. Alternative vantages of the difference of electronic densities of (M)-NP3H and movies of the difference of electronic densities of the relevant states **(*M*)-NP3H**. Computed ECD spectra of Molecular Fragments. Further details on the computations with the excitonic model.

Acknowledgments

D.A. acknowledges Fundación Ramón Areces (Spain) for funding his PostDoc position at ICCOM-CNR, Pisa. Computational resources provided by ThC2-Lab at ICCOM Pisa and by SCBI (Supercomputing and Bioinformatics) center of Universidad de Málaga are also acknowledged. C.N. thanks Sheldon and Dorothea Buckler for their generous support. Support for this research was provided by the U.S. Office of Naval Research under award No. N00014-16-1-2921 and the U.S. Department of Energy, under award No. DE-SC0014563. F.S and D.A. thanks Roberto Improta (IBB-CNR Napoli) for useful discussions.

References

1. Shen, Y.; Chen, C.-F. Helicenes: Synthesis and Applications. *Chem. Rev.* **2012**, *112*, 1463−1535.
2. Gingras, M. One Hundred Years of Helicene Chemistry. Part 1: Non-stereoselective Syntheses of Carbohelicenes. *Chem. Soc. Rev.* **2013**, *42*, 968−1006.
3. Gingras, M.; Felix, G.; Peresutti, R. One Hundred Years of Helicene Chemistry. Part 2: Stereoselective Syntheses and Chiral Separations of Carbohelicenes. *Chem. Soc. Rev.* **2013**, *42*, 1007−1050.
4. Gingras, M. One Hundred Years of Helicene Chemistry. Part 3: Applications and Properties of Carbohelicenes. *Chem. Soc. Rev.* **2013**, *42*, 1051−1095.
5. Brandt, J. R.; Salerno, F.; Fuchter, M. J. The Added Value of Small-molecule Chirality in Technological Applications. *Nat. Rev. Chem.* **2017**, *1*, 45.
6. Pop, F.; Zigon, N.; Avarvari, N. Main-Group-Based Electro- and Photoactive Chiral Materials. *Chem. Rev.* **2019**, *119*, 8435−8478.
7. Nakai, Y.; Mori, T.; Inoue, Y. Theoretical and Experimental Studies on Circular Dichroism of Carbo[n]Helicenes. *J. Phys. Chem. A* **2012**, *116*, 7372–7385.
8. Berezhnaia, V.; Roy, M.; Vanthuyne, N.; Villa, M.; Naubron, J. V.; Rodriguez, J.; Coquerel, Y.; Gingras, M. Chiral Nanographene Propeller Embedding Six Enantiomerically Stable [5]Helicene Units. *J. Am. Chem. Soc.* **2017**, *139*, 18508–18511.
9. Zhu, Y.; Xia, Z.; Cai, Z.; Yuan, Z.; Jiang, N.; Li, T.; Wang, Y.; Guo, X.; Li, Z.; Ma, S.; et al. Synthesis and Characterization of Hexapole [7]Helicene, A Circularly Twisted Chiral Nanographene. *J. Am. Chem. Soc.* **2018**, *140*, 4222–4226.
10. Liu, G.; Koch, T.; Li, Y.; Doltsinis, N. L.; Wang, Z. Nanographene Imides Featuring Dual-Core Sixfold [5]Helicenes. *Angew. Chem. Int. Ed.* **2019**, *58*, 178–183.
11. Meng, D.; Liu, G.; Xiao, C.; Shi, Y.; Zhang, L.; Jiang, L.; Baldridge, K. K.; Li, Y.; Siegel, J. S.; Wang, Z. Corannurylene Pentapetalae. *J. Am. Chem. Soc.* **2019**, *141*, 5402–5408.

12. Cruz, C. M.; Márquez, I. R.; Castro-Fernández, S.; Cuerva, J. M.; Maçôas, E.; Campaña, A. G. A Triskelion-Shaped Saddle–Helix Hybrid Nanographene. *Angew. Chem. Int. Ed.* **2019**, *58*, 8068–8072.

13. Roy, M.; Berezhnaia, V.; Villa, M.; Vanthuyne, N.; Giorgi, M.; Naubron, J. V.; Poyer, S.; Monnier, V.; Charles, L.; Carissan, Y.; et al. Stereoselective Syntheses, Structures, and Properties of Extremely Distorted Chiral Nanographenes Embedding Hextuple Helicenes. *Angew. Chem. Int. Ed.* **2020**, *59*, 3264–3271.

14. Schuster, N. J.; Paley, D. W.; Jockusch, S.; Ng, F.; Steigerwald, M. L.; Nuckolls, C. Electron Delocalization in Perylene Diimide Helicenes. *Angew. Chem. Int. Ed.* **2016**, *55*, 13519–13523.

15. Schuster, N. J.; Hernández Sánchez, R.; Bukharina, D.; Kotov, N. A.; Berova, N.; Ng, F.; Steigerwald, M. L.; Nuckolls, C. A Helicene Nanoribbon with Greatly Amplified Chirality. *J. Am. Chem. Soc*. **2018**, 140, 6235−6239.

16. Liu, B.; Böckmann, M.; Jiang, W.; Doltsinis, N. L.; Wang, Z. Perylene Diimide-Embedded Double [8]Helicenes. *J. Am. Chem. Soc.* **2020**, *142*, 7092–7099.

17. McCormick, T. M.; Bridges, C. R.; Carrera, E. I.; Dicarmine, P. M.; Gibson, G. L.; Hollinger, J.; Kozycz, L. M.; Seferos, D. S. Conjugated Polymers: Evaluating DFT Methods for More Accurate Orbital Energy Modeling. Macromolecules **2013**, *46* (10), 3879–3886.

18. Guido, C. A.; Knecht, S.; Kongsted, J.; Mennucci, B. Benchmarking Time-Dependent Density Functional Theory for Excited State Geometries of Organic Molecules in Gas-Phase and in Solution. *J. Chem. Theory Comput.* **2013**, *9* (5), 2209–2220.

19. Jacquemin, D.; Adamo, C. Computational Molecular Electronic Spectroscopy with TD-DFT. In *Density-Functional Methods for Excited States*; 2015; pp 347–375.

20. Aranda, D.; Cerezo, J.; Pescitelli, G.; Avila Ferrer, F. J.; Soto, J.; Santoro, F. A Computational Study of the Vibrationally-Resolved Electronic Circular Dichroism Spectra of Single-Chain Transoid and Cisoid Oligothiophenes in Chiral Conformations. *Phys. Chem. Chem. Phys.* **2018**, *20*, 21864–21880.

21. Karsten, B. P.; Bijleveld, J. C.; Viani, L.; Cornil, J.; Gierschner, J.; Janssen, R. A. J. Electronic Structure of Small Band Gap Oligomers Based on Cyclopentadithiophenes and Acceptor Units. *J. Mater. Chem.* **2009**, *19*, 5343–5350.

22. Erdmann, T.; Fabiano, S.; Milián-Medina, B.; Hanifi, D.; Chen, Z.; Berggren, M.; Gierschner, J.; Salleo, A.; Kiriy, A.; Voit, B et al. Naphthalenediimide Polymers with Finely Tuned In-Chain π-Conjugation: Electronic Structure, Film Microstructure, and Charge Transport Properties. *Adv. Mater.* **2016**, *28*, 9169–9174.

23. Yanai, T.; Tew, D. P.; Handy, N. C. A New Hybrid Exchange-Correlation Functional Using the Coulomb-Attenuating Method (CAM-B3LYP). *Chem. Phys. Lett.* **2004**, *393*, 51–57.

24. Grimme, S.; Antony, J.; Ehrlich, S.; Krieg, H. A Consistent and Accurate Ab Initio Parametrization of Density Functional Dispersion Correction (DFT-D) for the 94 Elements H-Pu. *J. Chem. Phys.* **2010**, *132*, 154104.

25. Johnson, E. R.; Becke, A. D. A Post-Hartree-Fock Model of Intermolecular Interactions: Inclusion of Higher-Order Corrections. *J. Chem. Phys.* **2006**, *124*, 174104.

26. Grimme, S.; Ehrlich, S.; Goerigk, L. Effect of the Damping Function in Dispersion Corrected Density Functional Theory. *J. Comput. Chem.* **2011**, *32*, 1456–1465.

27. Hellou, N.; Jahier-Diallo, C.; Baslé, O.; Srebro-Hooper, M.;Toupet, L.; Roisnel, T.; Caytan, E.; Roussel, C.; Vanthuyne, N.;Autschbach, J. et al. Electronic and Chiroptical Properties of Chiral Cycloiridiated Complexes Bearing Helicenic NHC Ligands. *Chem.Commun*. **2016**, 52, 9243−9246.

28. Shen, C.; Loas, G. h.; Srebro-Hooper, M.; Vanthuyne, N.; Toupet, L.; Cador, O.; Paul, F.; López Navarrete, J. T.; Ramírez, F. J.; Nieto-Ortega, B. et al. Iron Alkynyl Helicenes: Redox-triggered Chiroptical Tuning in the IR and Near-IR Spectral Regions and Suitable for Telecommunications Applications. *Angew. Chem., Int. Ed*. **2016**, 55,8062−8066.

29. Isla, H.; Srebro-Hooper, M.; Jean, M.; Vanthuyne, N.; Roisnel,T.; Lunkley, J. L.; Muller, G.; Williams, J. A. G.; Autschbach, J.;Crassous, J. Conformational Changes and Chiroptical Switching of Enantiopure bis-Helicenic Terpyridine upon Zn^{2+} Binding. *Chem.Commun*. **2016**, 52, 5932−5935.

30. Nakai, Y.; Mori, T.; Inoue, Y. Circular Dichroism of (di)methyl- and Diaza[6]helicenes. A Combined Theoretical and Experimental Study. *J. Phys. Chem. A* **2013**, 117, 83−93.

31. Tanaka, H.; Kato, Y.; Fujiki, M.; Inoue, Y.; Mori, T. Combined Experimental and Theoretical Study on Circular Dichroism and Circularly Polarized Luminescence of Configurationally Robust D3-symmetric Triple Pentahelicene. *J. Phys. Chem. A* **2018**, 122, 7378−7384.

32. Aharon, T.; Caricato, M. Configuration Space Analysis of the Specific Rotation of Helicenes. *J. Phys. Chem. A* **2019**, 123, 4406−4418.

33. Gaussian 16, Revision B.01, Frisch, M. J.; Trucks, G. W.; Schlegel, H. B.; Scuseria, G. E.; Robb, M. A.; Cheeseman, J. R.; Scalmani, G.; Barone, V.; Petersson, G. A.; Nakatsuji, H.; Li, X.; et al. Gaussian, Inc., Wallingford CT, 2016.

34. Aidas, K.; Angeli, C.; Bak, K. L.; Bakken, V.; Bast, R.; Boman, L.; Christiansen, O.; Cimiraglia, R.; Coriani, S.; Dahle, P.; et al. The Dalton Quantum Chemistry Program System. *Wiley Interdisciplinary reviews - Computational Molecular Science* **2014**, 4, 269-284.

35. Martin, R. L. Natural Transition Orbitals. J. Chem. Phys. 2003, 118, 4775-4777.

36. Avila Ferrer, F. J.; Santoro, F. Comparison of Vertical and Adiabatic Harmonic Approaches for the Calculation of the Vibrational Structure of Electronic Spectra. *Phys. Chem. Chem. Phys.* **2012**, *14*, 13549–13563.

37. F. Santoro, J. Cerezo. FCclasses3, a code for vibronic calculations. available upon request. **2019**.

38. Liu, Y.; Cerezo, J.; Mazzeo, G.; Lin, N.; Zhao, X.; Longhi, G.; Abbate, S.; Santoro, F. (2016). Vibronic Coupling Explains the Different Shape of Electronic Circular Dichroism and of Circularly Polarized Luminescence Spectra of Hexahelicenes. *J. Chem. Theory Comput.* **2016**, 12, 2799-2819.

39. Liu, Y.; Xu, Q.; Sun, J.; Wang, L.; He, D.; Wang, M.; Yang, C. Insights for Vibronic Effects on Spectral Shapes of Electronic Circular Dichroism and Circularly Polarized Luminescence of Aza[7]helicene. *Spectroc. Acta Part A* **2020**, 118475.

40. Jurinovich, S.; Cupellini, L.; Guido, C. A.; Mennucci, B. EXAT: Excitonic Analysis Tool. *J. Comput. Chem.* **2018**, *39*, 279–286.

41. Laurent, A. D.; Jacquemin, D. TD-DFT Benchmarks: A Review. *Int. J. Quantum Chem*. **2013**, *113*, 2019–2039.

42. Tomasi, J.; Mennucci, B.; Cammi, R. Quantum Mechanical Continuum Solvation Models. *Chem. Rev.* **2005**, *105*, 2999–3093.

43. Bak, K. L.; Hansen, A. E.; Ruud, K.; Helgaker, T.; Olsen, J.; Jørgensen, P. *Ab Initio* Calculation of Electronic Circular Dichroism for Trans-Cyclooctene Using London Atomic Orbitals. *Theor. Chim. Acta* **1995**, *90*, 441–458.

44. The PyMOL Molecular Graphics System, Version 2.7, Schrödinger, LLC.

45. Tanaka, H.; Ikenosako, M.; Kato, Y.; Fujiki, M.; Inoue, Y.; Mori, T. Symmetry-Based Rational Design for Boosting Chiroptical Responses. *Commun. Chem.* **2018**, *1*, 38.

46. Laarhoven, W. H.; De Jong, M. H. Photodehydrocyclizations of Stilbene-Like Compounds. VIII. Synthesis of Hexaheliceno[3,4-C.]hexahelicene. *Recl. Trav. Chim. Pays-Bas* **1973**, *92*, 651–657.

47. Schuster, N. J.; Joyce, L. A.; Paley, D. W.; Ng, F.; Steigerwald, M. L.; Nuckolls, C. The Structural Origins of Intense Circular Dichroism in a Waggling Helicene Nanoribbon. *J. Am. Chem. Soc.* **2020**, *142*, 7066–7074.

48. Xiao, X.; Pedersen, S. K.; Aranda, D.; Yang, J.; Wiscons, R. A.; Pittelkow, M.; Steigerwald, M. L.; Santoro, S.; Schuster, N. J.; Nuckolls, C. Chirality Amplified: Long, Discrete Helicene Nanoribbons. *J. Am. Chem. Soc*. DOI:10.1021/jacs.0c11260.

For Table of Contents Only